

Small-polaron mediated recombination in titanium dioxide from first principles

James A. Quirk^{✉*} and Keith P. McKenna^{✉†}

School of Physics, Engineering and Technology, University of York, York, YO10 5DD, United Kingdom



(Received 21 November 2022; accepted 6 March 2023; published 1 May 2023)

Nonradiative recombination leads to losses in efficiency in optoelectronic devices such as photovoltaic cells and light-emitting diodes. Charges trapped at point defects or self-trapped as a small polaron may act as recombination centers. Using various phases of titanium dioxide as an example, we provide first-principles predictions that small hole polarons in the bulk of the crystal would exhibit significant rates of recombination with electrons in the conduction band. However, small hole polarons trapped at a model grain boundary are predicted to have much higher nonradiative recombination rates, which can be attributed to softer phonon modes in the vicinity of the boundary as well as greater electron-phonon coupling. These findings have ramifications in materials other than titanium dioxide, and we propose strategies to reduce the degree of recombination that would occur at grain boundaries.

DOI: [10.1103/PhysRevResearch.5.023072](https://doi.org/10.1103/PhysRevResearch.5.023072)

I. INTRODUCTION

The recombination of photoexcited charge carriers plays a crucial role in determining the properties of semiconducting materials with relevance to applications in photovoltaics, photocatalysis, and photoelectrochemistry. The trapping of electrons or holes at various defects in materials including point defects (such as vacancies, impurities, and interstitials) and extended defects (such as dislocations [1,2], surfaces [3,4], and grain boundaries [5–7]) is known to enhance rates of recombination. A trapped electron or hole may recombine with its oppositely charged counterpart in either a radiative process (through the emission of a photon) or a nonradiative process (through the emission of phonons). In highly polarizable materials, the trapping of charge carriers in the perfect bulk lattice is also possible, leading to the formation of small polarons, which are quasiparticles consisting of a charge carrier coupled to a distortion in the crystal [8]. In principle, small polarons generated under photoexcitation of a semiconductor may also act as recombination centers but such processes are rarely considered and there are many open questions. For example, do small polarons facilitate radiative and nonradiative recombination and what factors influence their relative rates? In the former case, can the associated photoluminescence be disentangled from that of other intrinsic and extrinsic defects?

TiO₂ is an archetypal example of an optoelectronic material that is sufficiently polarizable for small polarons to form.

Depending on the polymorph in question, either electron, hole, or both types of small polarons can form [9,10]. TiO₂ has seen extensive study due to its wide range of potential applications; including as an electron transport layer in solar cells [11] and as a photocatalyst for removing harmful pollutants from the air and for the splitting of water for hydrogen production [12,13]. In particular, the anatase polymorph of TiO₂ has drawn significant interest due to its very high electron mobility, which can be attributed to it exhibiting favorable self-trapping of holes, but not of electrons [10]. A computational study has predicted that this behavior is also shared by the less-studied polymorphs, brookite and TiO₂(B) [9]. Despite the huge body of work, details of how charge carriers recombine in TiO₂ remain elusive. Recombination processes can be probed experimentally through photoluminescence (PL) spectroscopy, but it is extraordinarily challenging to disentangle recombination occurring at self-trapped charge carriers in bulk from recombination occurring at point or extended defects. There has been extensive work concerning anatase, but various mechanisms have been proposed regarding the competing radiative and nonradiative processes [14–16]. For other polymorphs, such as brookite and TiO₂(B), there are very few experimental results in the literature.

In this study, we present results of a first-principles investigation of radiative and nonradiative recombination in the bulk of three TiO₂ polymorphs where small hole polarons are predicted to be stable: anatase, brookite, and TiO₂(B). Standard density functional theory (DFT) approaches are not sufficient for modeling localized charges, so we employ a hybrid DFT approach where the fraction of Fock exchange we introduce is explicitly tailored for an accurate description of small polarons in TiO₂ by matching to a known constraint in exact DFT [9]. We investigate both radiative and nonradiative recombination and provide predicted PL lineshapes in order to aid comparison with experiment. We determine that self-trapped polarons in the bulk of these polymorphs would not lead to a significant degree of nonradiative recombination

*Present address: Chemistry Department, Newcastle University, Newcastle upon Tyne NE1 7RU, UK; james.quirk@newcastle.ac.uk
 †keith.mckenna@york.ac.uk

Published by the American Physical Society under the terms of the Creative Commons Attribution 4.0 International license. Further distribution of this work must maintain attribution to the author(s) and the published article's title, journal citation, and DOI.

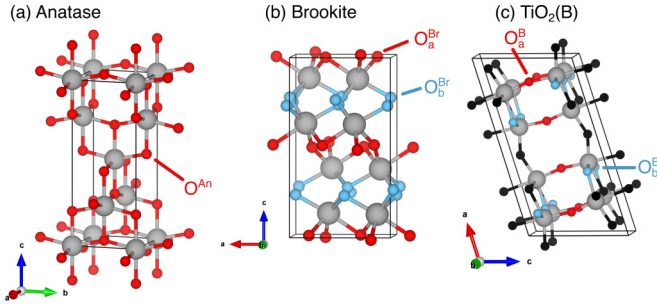


FIG. 1. Conventional unit cells of (a) anatase, (b) brookite, and (c) TiO₂(B). Large gray spheres are titanium and small spheres are oxygen. Oxygen sites where hole polarons can form are color coded and labeled in red and blue. Oxygen sites where hole polarons are not predicted to form are black.

and suggest that nonradiative recombination involving self-trapped holes predominantly occurs elsewhere in the crystal, such as at extended defects. This prediction is supported by the higher capture coefficients that we calculate for holes trapped in the vicinity of a grain boundary in anatase.

II. BACKGROUND AND THEORY

Physically speaking, a polaron consists of a charge carrier coupled to a cloud of virtual phonons that describe the lattice polarization induced by the presence of the carrier [17]. A standard DFT calculation does not explicitly contain any terms corresponding to these phonons, but the introduction of an excess charge carrier to a simulation supercell will introduce forces that correspond to the lattice distortion. Geometry optimization procedures can minimize these forces such that, given a suitable DFT functional and a sensible starting geometry, a standard DFT functional can correctly describe the geometry of a polaron at 0 K, so long as the polaron is small enough that it can be captured within the supercell. Vibrational effects can then be accounted for by treating nuclei classically within the Born-Oppenheimer approximation and considering how the total energy from DFT changes with ionic displacements [18–20].

All of the TiO₂ phases considered in this study are shown in Fig. 1. For anatase, there is only one distinct oxygen site with one corresponding polaron [Fig. 1(a)]. In brookite, there are two distinct oxygen sites each with an associated polaron, which we label O^{Br}_a and O^{Br}_b [Fig. 1(b)]. In TiO₂(B), there are four inequivalent oxygen sites, where only two will allow the formation of polarons, where we label these two sites O^B_a and O^B_b [Fig. 1(c)]. Note that O^B_a is two-coordinated, whereas all of the other sites are three-coordinated. In each phase, these hole polarons are used to tune a hybrid DFT functional such that it satisfies the generalized Koopmans' condition (GKC), which gives an expression for the ionization energy of a system of N electrons, $I(N)$, as

$$-I(N) \equiv E(N) - E(N - 1) = \epsilon_N(N), \quad (1)$$

where $E(N)$ is the total energy of an N electron system, and $\epsilon_i(N)$ is the i th eigenvalue of the N electron system. Such an approach has been shown to accurately reproduce experimental results [21–23] in molecular systems. In this work, we use

GKC-tuned fractions of Fock exchange of 10.5% for anatase and brookite, and 12.0% for TiO₂(B). A more complete description of this approach and of the polarons in each phase can be found in Ref. [9].

We model the recombination of a hole self-trapped on an oxygen with an electron in the conduction band ($O_0^+ + e^- \rightarrow O_0^0$). The procedures for determining simulated PL spectra [24] and electron capture coefficients [25] for radiative and nonradiative recombination, respectively, have been outlined by Alkauskas *et al.* For radiative recombination, the bulk of the work lies in calculating the spectral function, A , as a function of photon energy, $\hbar\omega$, as

$$A(\hbar\omega) = \sum_{m,n} w_m(T) |\langle \chi_{em} | \chi_{gn} \rangle|^2 \times \delta(\Delta E + \hbar\omega_{em} - \hbar\omega_{gn} - \hbar\omega). \quad (2)$$

The sum runs over all vibrational levels with energies $\hbar\omega_{em}$ and $\hbar\omega_{gn}$ for the excited and ground state, respectively, where $w_m(T)$ is the thermal occupation of the excited state at temperature T and where $\chi_{e,g}$ are ionic wave functions. ΔE is the difference in energy between the excited and ground states, which we take from the charge transition level (CTL) of the defect. To allow numerical evaluation, the δ function is replaced with a Gaussian smearing function. For nonradiative recombination, we wish to calculate the capture coefficient, $C(T)$, which is given by

$$C(T) = V \frac{2\pi}{\hbar} g W_{if}^2 \sum_m w_m(T) \sum_n |\langle \chi_{em} | Q | \chi_{gn} \rangle|^2 \times \delta(\Delta E + \hbar\omega_{em} - \hbar\omega_{gn}). \quad (3)$$

All terms in this equation have the same meaning as in Eq. (2), aside from the newly appearing terms of V , the volume of the simulation supercell; g , the degeneracy of the defect, which is one for all of the polarons we consider; Q , an appropriately chosen configuration coordinate, which shall be outlined later when we discuss the practicalities of the calculation; and W_{if} , the electron-phonon coupling term which, in this problem, can be given by

$$W_{if} = (\epsilon_f - \epsilon_i) \left\langle \psi_i \left| \frac{\partial \psi_f}{\partial Q} \right. \right\rangle, \quad (4)$$

where ϵ_i and ϵ_f are the single-particle energy eigenvalues of the single-particle orbitals ψ_i and ψ_f , obtained by solving the Kohn-Sham equations. For a nondegenerate state such as the polarons we are considering, the derivative $\partial \psi_f / \partial Q$ can be calculated numerically using finite differences as outlined in Ref. [25].

Examining Eqs. (2) and (3), we can see that both problems are similar in that they require the calculation of overlap integrals between the ionic wave functions, χ . Essentially, the majority of the required work follows the same procedure

- (1) Determine the ground- and excited-state potential energy surface.
- (2) Determine the ionic wave functions corresponding to these potential energy surfaces.
- (3) Calculate the required overlap integrals between the ionic wave functions in order to yield the quantities of interest.

TABLE I. Key values for the polarons studied in this work: nonradiative recombination barrier (E_b^{NR}); the calculated ionization barrier (E_b^{I}) and range of activation energies (E_{act}) for hole polaron hopping in bulk anatase, brookite, and $\text{TiO}_2(\text{B})$ taken from Ref. [30]; total mass-weighted distortions (ΔQ); electron-phonon coupling matrix elements (W_{if}); and effective frequencies for the ground ($\hbar\Omega_g$) and excited state ($\hbar\Omega_e$).

Site	E_b^{NR} (eV)	E_b^{I} (eV)	E_{act} (eV)	ΔQ (amu $^{\frac{1}{2}}$ Å)	W_{if} (eV amu $^{-\frac{1}{2}}$ Å $^{-1}$)	$\hbar\Omega_g$ (meV)	$\hbar\Omega_e$ (meV)	S_g
O ^{An}	0.74	0.24	0.12–0.36	2.16	2.2×10^{-4}	47	41	20.4
O ^{Br} _a	1.57	0.12	0.08–0.33	2.06	33.9×10^{-4}	44	34	17.0
O ^{Br} _b	1.67	0.10	0.08–0.33	2.30	66.8×10^{-4}	39	29	18.9
O ^B _a	1.01	0.42	0.04–0.39	2.16	4.6×10^{-4}	50	39	23.3
O ^B _b	1.40	0.53	0.04–0.41	2.20	0.2×10^{-4}	45	40	22.7
O ^{An} _{GB-3c}	0.23	0.50		2.99	65.4×10^{-4}	34	32	37.8
O ^{An} _{GB-2c}	0.40	0.27		2.60	17.2×10^{-4}	39	33	30.2

Normally, describing the potential energy surface (PES) would not be trivial as it would require the consideration of all vibrational degrees of freedom. However, the phonons that couple most strongly to the lattice distortion are the ones that contribute most to the electron-phonon coupling, where the strength of the electron-phonon coupling can be quantified by the Huang-Rhys factor, S , which corresponds to the average number of phonons created in a vertical transition and which is given by

$$S_{e,g} = \frac{\Delta E_{e,g}^{\text{rel}}}{\hbar\Omega_{e,g}}, \quad (5)$$

where $\Delta E_{e,g}^{\text{rel}}$ are the relaxation energies associated with a vertical transition to the excited or ground states. In the case of defects with strong electron-phonon coupling ($S \gg 1$), it has been shown numerically that it is a good approximation to employ a one-dimensional (1D) model where all the vibrational degrees of freedom are replaced by a single, special phonon mode that maps the excited state onto the ground state [24]. We are concerned with Huang-Rhys factor of the final state, S_g , which corresponds to the vertical transition from the excited state to the ground state and which is found to be $\gg 1$ for all polarons we consider (Table I). In this 1D model, a generalized configuration coordinate, Q , is defined as

$$Q^2 = \sum_i M_i [R_i(t) - R_i(0)]^2, \quad (6)$$

where M_i are the atomic masses and $R_i(t)$ are the atomic coordinates at configuration t , where $t = 0$ corresponds to the geometry of the pristine bulk and $t = 1$ corresponds to an optimized polaron geometry. The value of Q at the polaron geometry is referred to as ΔQ .

Now, for each polaron, a PES is produced for both the ground state (a neutrally charged system corresponding to O_0^0) and the excited state (a positively charged system corresponding to O_0^+) by calculating single-point energies for range of interpolated images between $-\Delta Q$ to $2\Delta Q$ in increments of $0.1\Delta Q$. The energy difference between the minima of each PES is taken from the charge transition level. This yields

a 1D configuration coordinate diagram from which various quantities of interest can be extracted. These quantities are illustrated in a schematic example (Fig. 2). Next, the 1D Schrödinger equation is solved in order to yield the ionic wave functions. This, as well as the subsequent overlap integrals, are achieved using the CarrierCapture.jl code [26], which uses splines to fit to the calculated points along the PES, enabling the study of recombination at defects that may have an anharmonic PES. CarrierCapture.jl has been used extensively to elucidate recombination processes at defects in photovoltaic materials [27–29].

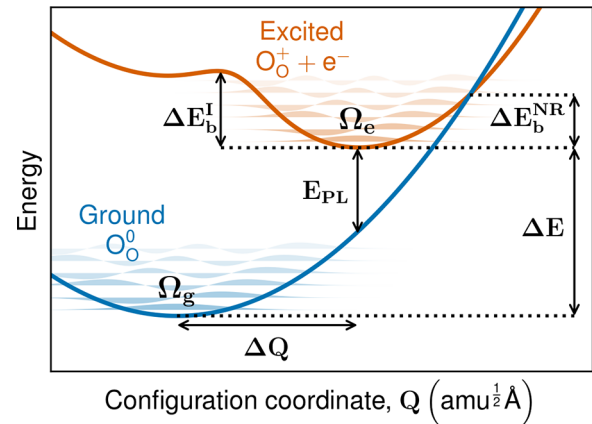


FIG. 2. Schematic example of a configuration coordinate diagram for a hole polaron in TiO_2 . The potential energy surfaces for the excited and the ground state are quantum oscillators with effective frequencies of Ω_e and Ω_g , respectively. The difference in energy between the curves is ΔE , which is taken from the charge transition level. The difference in the configuration coordinate between lowest energy geometries of the excited state and the ground state is given by ΔQ . The crossing point of each curve corresponds to the barrier to nonradiative recombination, E_b^{NR} . The charge may also delocalize, causing the excited system to take on the geometry of the ground state; the barrier to this ionization process is labeled as E_b^{I} . Also shown is an idealized value of the peak photoluminescent emission energy, E_{PL} , at low temperatures.

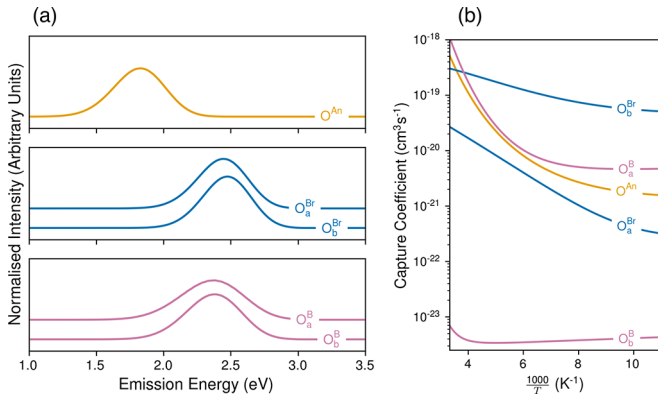


FIG. 3. (a) The simulated PL lineshapes associated each of the considered hole polarons. Curves have been offset vertically for brookite and $TiO_2(B)$ in the interest of clarity. (b) Calculated capture coefficients for each of the hole polarons. Capture coefficients are extremely small between 50 to 300 K and do not indicate significant nonradiative recombination in bulk.

III. RESULTS AND DISCUSSION

We evaluate the profile of the PL lineshapes at 77 K (liquid nitrogen temperature) [Fig. 3(a)]. For now, we shall focus on anatase, where we obtain a PL peak, E_{PL} , of 1.86 eV, which is a slight underestimate of experimentally reported value of around 2.2 eV [31–34]. It should be noted that while the functional we use has been carefully parameterized to describe small polarons accurately, it has a tendency to underestimate experimental band gaps slightly, predicting a gap of 2.94 eV compared to experimental values of around 3.20 eV. An incorrect band gap limits the degree to which the simulated PL peaks, E_{PL} , can be quantitatively compared to experiment. In fact, even functionals which have been tuned to reproduce the experimental band gap do not necessarily produce the correct value of E_{PL} [24]. Nevertheless, if we make the assumption that absorption is dominated by the transition from the VBM to CBM, then we can then define the Stokes shift as $\Delta E_{PL} = E_g - E_{PL}$, where E_g is the calculated band gap of the relevant polymorph containing the polaron. In the case of anatase, we find that our calculated value of $\Delta E_{PL} = 1.08$ eV is in reassuring agreement with experimental observations which generally range from around 0.9 to 1.3 eV [31–34].

Brookite and $TiO_2(B)$ present a more troublesome picture than anatase as there are far fewer published studies and, of those that do exist, the focus is often on samples with unusual morphology or a high concentration of dopants and defects; both properties can significantly reduce the optical band gap by introducing states either above or below the VBM and CBM, respectively. The experimental consensus from PL experiments is that brookite has a band gap of around 3.1 to 3.4 eV [35–37]. This value is comparable to the experimental consensus for the band gap of anatase, which is at odds with theoretical predictions that brookite should have a significantly wider band gap than anatase [9,38], specifically greater by 0.26 eV in this study. PL peaks are similarly hard to pin down, with a common value being around 3.0 eV [36,37]. For $TiO_2(B)$, the range of band gaps of reported band gaps is even wider, going from 2.9 to 3.6 eV [39–42]. As might be

expected, photoluminescent peaks range from around 1.9 to 2.9 eV and are variably attributed to self-trapped charges and oxygen vacancies [42–44]. Plainly, the experimental evidence for both brookite and $TiO_2(B)$ is too inconsistent to make a proper comparison with our simulations, but we provide our results in the hope that they may aid interpretation of future experiments. Notably, we predict that the peak emission for a given polaron is almost identical across different sites in the same phase, indicating that we should expect only one peak for radiative recombination of bulk polarons.

Regarding nonradiative recombination, we find that all the considered self-trapped holes in bulk have very large barriers to nonradiative recombination (marked as E_b^{NR} on Fig. 2 and determined by the crossing point of the PESs) with correspondingly tiny capture coefficients (generally within the range of around 10^{-21} to $10^{-18} cm^3 s^{-1}$) and therefore would not be likely to undergo nonradiative recombination. However, PL experiments performed on anatase have determined that some proportion of the recombination occurring at self-trapped polarons is nonradiative [14–16], with deep hole-trapping states being explicitly implicated in one study [45]. We propose that the majority of this observed nonradiative recombination is not occurring in the pristine bulk, but instead occurs in the vicinity of other defects; this could mean the recombination of a hole in the valence band with an electron trapped at a defect, or it could mean a hole trapped at a defect recombining with an electron in the conduction band. A previous computational study in our group using the same functional determined that the barriers to hole polaron hopping and ionization in these polymorphs are significantly lower than the barriers to nonradiative recombination in the bulk [30], suggesting that photogenerated holes would be mobile at relatively low temperatures. This would allow the holes to migrate through the bulk until they encounter a deeper trap at, for example, grain boundaries or surfaces. These deeper traps would have a charge transition level (CTL) closer to the middle of the band gap and would likely have a lower barrier and, making them more conducive to nonradiative recombination. This supports previous experimental work which demonstrates that surfaces contribute to a large proportion of the nonradiative recombination that occurs in TiO_2 [15].

Figure 3(b) appears to show an anomaly in the form of O_b^B , which has a capture coefficient far lower than all of the other sites. This could, in part, be attributed to O_a^B having a lower barrier to nonradiative recombination, E_b^{NR} , when compared to the O_b^B . However, both the O_a^{Br} and O_b^{Br} sites in brookite have larger barriers than O_b^B and yet still show much larger capture coefficients. Clearly, it is not only the barrier to nonradiative recombination that is important in determining the capture coefficient; these results highlight the role of the electron-phonon coupling term, W_{if} , in nonradiative recombination. Site O_b^B has an electron-phonon coupling term that is around an order of magnitude lower than the electron-phonon coupling term compared to site O_a^B , which then leads to a far lower capture coefficient. Such a large difference between two sites in the same material should not be surprising given that they are in significantly different bonding environments, with O_b^B being three-coordinated and O_a^B being two-coordinated. This raises a question regarding extended defects: Aside from differences in the electronic structure and trapping energies,

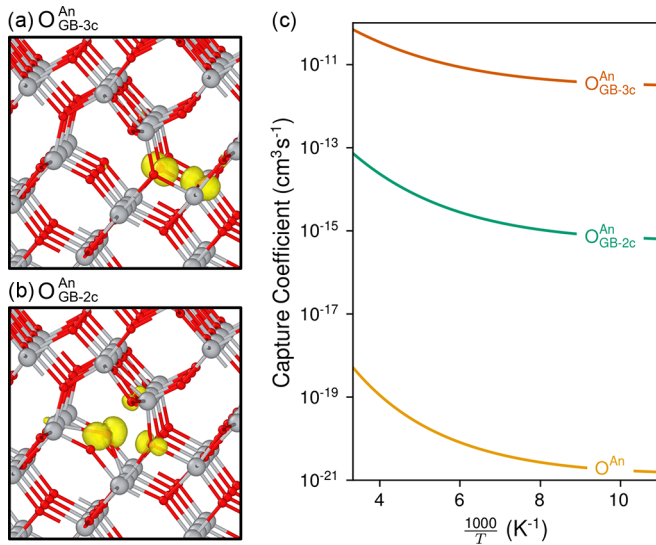


FIG. 4. Structural models and spin density isosurfaces (displayed at $0.01 a_0^{-3}$) associated with hole polarons at the (a) O_{GB-3c}^{An} and (b) O_{GB-2c}^{An} sites in the $\Sigma 5\{103\}$ GB in anatase. (c) Calculated capture coefficients for each of the hole polarons in the vicinity of the anatase GB compared with a polaron in bulk anatase.

could the different bonding environments at grain boundaries be responsible for increased rates of nonradiative recombination?

Previous studies using the same hybrid-DFT functional have shown that, in general, grain boundaries only weakly perturb the electronic structure of anatase, even if the boundary imposes a significantly different bonding environment on the atoms [7]. One example is the $\Sigma 5\{103\}$ anatase grain boundary [46], which exhibits no change to the band gap and no trap states in the equilibrium geometry, but which does exhibit a mixture of three- and two-coordinated O sites. This provides a convenient case study, as it allows us to directly investigate the effects that different coordination environments have on the carrier recombination in anatase, without the analysis being muddled by the effects of severe perturbations to local electronic structure. Lowest energy configurations are identified for a hole polaron trapped at the three-coordinated grain boundary site that we label O_{GB-3c}^{An} [Fig. 4(a)] and a two-coordinated grain boundary site that we label O_{GB-2c}^{An} [Fig. 4(b)].

We find that the capture coefficients for a polaron trapped at either of these grain boundary sites are significantly higher than for a polaron trapped in the bulk [Fig. 4(c)]. This is, in part, due to both GB sites having a much greater value for electron-phonon coupling term, W_{if} , but is also due to lower barriers to recombination. The explanation for the lower barrier in O_{GB-3c}^{An} is straightforward as it has a formation energy that is 0.27 eV more favorable than the polaron in bulk, which leads to a CTL closer to the middle of the gap which brings the PES for the ground and excited states closer together. However, the formation energy of O_{GB-2c}^{An} is only slightly more favorable than the bulk (by around 0.02 eV) and so has a similar CTL, yet we find that barrier to recombination is much lower. This can be understood by considering the effective vibrational frequencies of the trap, $\hbar\Omega_{\{e,g\}}$, which are

defined as

$$\hbar\Omega_{\{e,g\}} = \frac{\partial^2 E_{\{e,g\}}}{\partial Q^2}, \quad (7)$$

and are shown in Table I and Fig. 2. The values of $\hbar\Omega_{\{e,g\}}$ for O_{GB-2c}^{An} correspond to significantly lower energies than for O^{An} , indicating that the phonon modes associated with the traps at the boundary are softer and easier to activate, even at lower temperatures. This leads to the trap at the boundary having a lower barrier to recombination, despite the formation energy of the trap being almost identical to the bulk-like trap.

These effects are unlikely to be unique to anatase and will have ramifications across a broad range of materials and applications. For example, there is evidence of increased nonradiative recombination in the vicinity of grain boundaries of methylammonium lead iodide (MAPI) [47] and CdTe [48]. This may not be entirely due to an increased density of point defects near the boundary due to segregation or even the depth of the traps at these defects, but may also be due to the increased capture coefficients due to the softer phonons in the vicinity of the GB structure itself, along with a greater degree of electron-phonon coupling at the boundary. Furthermore, the intrinsically pathological nature of recombination at grain boundaries will be further complicated by changes to electronic structure at the boundary; the $\Sigma 5\{103\}$ was chosen for this study due to the convenient feature of having an unchanged band gap, but not all boundaries will be so ideal. For example, a material may exhibit a narrowed band gap in the vicinity of the GB due to the CBM being lower in energy [49]. In this case, we should expect excess electrons to segregate towards the boundary. A small hole polaron formed at such a boundary should then also be expected to show increased rates of nonradiative recombination due to a greater overlap between the electron and holes, in addition to the increased electron-phonon coupling. Conversely, consider a system in which band gaps are wider at the boundary [50]. Now, we would expect that an introduced electron would preferentially segregate away from the boundary and therefore the recombination at the boundary would be lowered due to the decreased overlap between the carriers, which are now occupying different regions of space.

The latter example of a widened band gap leading to increased carrier separation and decreased carrier recombination highlights the importance of carrier separation. In fact, good carrier separation is so important that even a material with comparatively poor optical absorption can outperform a material with good optical absorption, so long as the poor absorber shows better charge separation [45]. Improving carrier separation to improve photovoltaic efficiency can be achieved by introducing a heterogeneous interface (for example, CdSe/CdS core/shell nanoparticles [51,52]) but it can also be achieved at grain boundaries within a material by utilizing dopants that segregate to boundaries and create a space-charge region that encourages charge separation (for example, CdTe solar cells doped with Cl) [53]. We suggest that a focus should be placed on engineering grain boundaries to enhance carrier separation in order to prevent carriers having the opportunity to recombine at all,

given the fact that grain boundaries can significantly enhance recombination.

IV. CONCLUSION

In summary, we have performed first-principles calculations to determine nonradiative recombination rates of electrons with small hole polarons in various phases of TiO_2 . We predict that recombination is extremely slow in bulk, but that grain boundaries can increase recombination rates due to the presence of softer phonon modes and an increase in the degree of electron-phonon coupling. We suggest that nonradiative recombination at grain boundaries could be reduced by doping strategies that focus on increasing the degree of carrier separation that occurs at the boundary. This study focuses only on small polarons, yet large polarons are also known to play a significant role in recombination in, for example, organic-inorganic halide perovskite devices [54,55]. A recent theoretical development capable of describing both small and large polarons at all couplings [20] may be able to provide an avenue into studying the effects grain boundaries have on recombination mediated by polarons at different scales.

ACKNOWLEDGMENTS

K.P.M. acknowledges support from EPSRC (Grants No. EP/P006051/1 and No. EP/P023843/1). This work made use of the facilities of Archer, the UK's national high-performance computing service, via our membership in the UK HPC Materials Chemistry Consortium, which is funded by EPSRC (Grants No. EP/L000202 and No. EP/R029431). This work also made use of the Viking Cluster, which is a high-performance computer facility provided by the

University of York. All data created during this research are available by request from the University of York Research database [56].

APPENDIX: COMPUTATIONAL METHODS

All first-principles calculations are carried out using the implementation of hybrid DFT within CP2K [57]. We employ a version of hybrid DFT where long-range HF exchange integrals are truncated, referred to as $\text{PBE}\alpha\text{-TC-LRC}$ [58,59], where we determine that a truncation radius of 6 \AA is well converged with regards to lattice parameters and band gaps. We use a fraction of Fock exchange that ensures that the generalized Koopmans' condition (GKC) is obeyed to within 0.05 eV in the bulk of each material: 10.5% for anatase and brookite, and 12.0% for $\text{TiO}_2(\text{B})$.

The computational cost of hybrid calculations is reduced by the auxiliary density matrix method (ADMM) [60] in which exchange integrals are approximated through mapping onto smaller, more localized basis sets. We use triple- ζ basis sets optimized from molecular calculations (MOLOPT) [61] and Goedecker-Teter-Hutter pseudopotentials available within CP2K [62–64] for both titanium and oxygen, where the $3s$, $3p$, $3d$, and $4s$ electrons are considered valence for titanium and the $2s$ and $2p$ electrons are considered valence for oxygen. We use five multigrids with a relative cutoff of 60 Ry, the finest grid having a cutoff of 600 Ry. As CP2K only samples the Γ point, we converge properties with respect to supercell size as opposed to k -point sampling in reciprocal space. A detailed description of the convergence of all of these quantities for each of the phases considered here can be found in our previous work along with a more detailed description of our generalized Koopmans' condition-tuned functional for TiO_2 polymorphs [9].

-
- [1] T. Wosiński, Evidence for the electron traps at dislocations in GaAs crystals, *J. Appl. Phys.* **65**, 1566 (1989).
 - [2] E. Maras, M. Saito, K. Inoue, H. Jønsson, Y. Ikuhara, and K. P. McKenna, Determination of the structure and properties of an edge dislocation in rutile TiO_2 , *Acta Mater.* **163**, 199 (2019).
 - [3] S. K. Wallace and K. P. McKenna, Facet-dependent electron trapping in TiO_2 nanocrystals, *J. Phys. Chem. C* **119**, 1913 (2015).
 - [4] M. Setvin, C. Franchini, X. Hao, M. Schmid, A. Janotti, M. Kaltak, C. G. Van de Walle, G. Kresse, and U. Diebold, Direct View at Excess Electrons in TiO_2 Rutile and Anatase, *Phys. Rev. Lett.* **113**, 086402 (2014).
 - [5] K. P. McKenna and A. L. Shluger, First-principles calculations of defects near a grain boundary in MgO , *Phys. Rev. B* **79**, 224116 (2009).
 - [6] T. Leijtens, S. D. Stranks, G. E. Eperon, R. Lindblad, E. M. Johansson, I. J. McPherson, H. Rensmo, J. M. Ball, M. M. Lee, and H. J. Snaith, Electronic properties of meso-superstructured and planar organometal halide perovskite films: Charge trapping, photodoping, and carrier mobility, *ACS Nano* **8**, 7147 (2014).
 - [7] J. A. Quirk, V. K. Lazarov, and K. P. McKenna, Electronic properties of $\{112\}$ and $\{110\}$ twin boundaries in anatase TiO_2 , *Adv. Theory Simul.* **2**, 1900157 (2019).
 - [8] A. Stoneham, J. Gavartin, A. Shluger, A. Kimmel, D. M. Ramo, H. Rønnow, G. Aeppli, and C. Renner, Trapping, self-trapping, and the polaron family, *J. Phys.: Condens. Matter* **19**, 255208 (2007).
 - [9] A. R. Elmaslmane, M. B. Watkins, and K. P. McKenna, First-principles modeling of polaron formation in TiO_2 polymorphs, *J. Chem. Theory Comput.* **14**, 3740 (2018).
 - [10] T. Berger, M. Sterrer, O. Diwald, E. Knözinger, D. Panayotov, T. L. Thompson, and J. T. Yates, Light-induced charge separation in anatase TiO_2 particles, *J. Phys. Chem. B* **109**, 6061 (2005).
 - [11] B. O'Regan and M. Grätzel, A Low-Cost, High-efficiency solar cell based on dye-sensitized colloidal TiO_2 films, *Nature (London)* **353**, 737 (1991).
 - [12] A. Fujishima and K. Honda, Electrochemical photolysis of water at a semiconductor electrode, *Nature (London)* **238**, 37 (1972).

- [13] S. G. Kumar and L. G. Devi, Review on modified TiO₂ photocatalysis under UV/visible light: Selected results and related mechanisms on interfacial charge carrier transfer dynamics, *J. Phys. Chem. A* **115**, 13211 (2011).
- [14] L. Cavigli, F. Bogani, A. Vinattieri, L. Cortese, M. Colocci, V. Faso, and G. Baldi, Carrier recombination dynamics in anatase TiO₂ nanoparticles, *Solid State Sci.* **12**, 1877 (2010).
- [15] L. Cavigli, F. Bogani, A. Vinattieri, V. Faso, and G. Baldi, Volume versus surface-mediated recombination in anatase TiO₂ nanoparticles, *J. Appl. Phys.* **106**, 053516 (2009).
- [16] K. Wakabayashi, Y. Yamaguchi, T. Sekiya, and S. Kurita, Time-resolved luminescence spectra in colorless anatase TiO₂ single crystal, *J. Lumin.* **112**, 50 (2005).
- [17] C. Franchini, M. Reticcioni, M. Setvin, and U. Diebold, Polarons in materials, *Nat. Rev. Mater.* **6**, 560 (2021).
- [18] W. H. Sio, C. Verdi, S. Ponc e, and F. Giustino, Polarons from First Principles, without Supercells, *Phys. Rev. Lett.* **122**, 246403 (2019).
- [19] W. H. Sio, C. Verdi, S. Ponc e, and F. Giustino, *Ab initio* theory of polarons: Formalism and applications, *Phys. Rev. B* **99**, 235139 (2019).
- [20] J. Lafuente-Bartolome, C. Lian, W. H. Sio, I. G. Gurtubay, A. Eiguren, and F. Giustino, *Ab initio* self-consistent many-body theory of polarons at all couplings, *Phys. Rev. B* **106**, 075119 (2022).
- [21] M. Srebro and J. Autschbach, Does a molecule-specific density functional give an accurate electron density? The challenging case of the CuCl electric field gradient, *J. Phys. Chem. Lett.* **3**, 576 (2012).
- [22] M. Srebro and J. Autschbach, Tuned range-separated time-dependent density functional theory applied to optical rotation, *J. Chem. Theory Comput.* **8**, 245 (2012).
- [23] L. Kronik, T. Stein, S. Refaely-Abramson, and R. Baer, Excitation gaps of finite-sized systems from optimally tuned range-separated hybrid functionals, *J. Chem. Theory Comput.* **8**, 1515 (2012).
- [24] A. Alkauskas, J. L. Lyons, D. Steiauf, and C. G. Van de Walle, First-Principles Calculations of Luminescence Spectrum Line Shapes for Defects in Semiconductors: The Example of GaN and ZnO, *Phys. Rev. Lett.* **109**, 267401 (2012).
- [25] A. Alkauskas, Q. Yan, and C. G. Van de Walle, First-principles theory of nonradiative carrier capture via multiphonon emission, *Phys. Rev. B* **90**, 075202 (2014).
- [26] S. Kim, S. N. Hood, P. van Gerwen, L. D. Whalley, and A. Walsh, Carriercapture.jl: Anharmonic carrier capture, *J. Open Source Softw.* **5**, 2102 (2020).
- [27] S. R. Kavanagh, A. Walsh, and D. O. Scanlon, Rapid recombination by cadmium vacancies in CdTe, *ACS Energy Lett.* **6**, 1392 (2021).
- [28] S. Kim, J.-S. Park, S. N. Hood, and A. Walsh, Lone-pair effect on carrier capture in Cu₂ZnSnS₄ solar cells, *J. Mater. Chem. A* **7**, 2686 (2019).
- [29] S. Kim, S. N. Hood, and A. Walsh, Anharmonic lattice relaxation during nonradiative carrier capture, *Phys. Rev. B* **100**, 041202(R) (2019).
- [30] J. J. Carey, J. A. Quirk, and K. P. McKenna, Hole polaron migration in bulk phases of TiO₂ using hybrid density functional theory, *J. Phys. Chem. C* **125**, 12441 (2021).
- [31] N. Hosaka, T. Sekiya, and S. Kurita, Excitonic state in anatase TiO₂ single crystal, *J. Lumin.* **72-74**, 874 (1997).
- [32] H. Tang, H. Berger, P. Schmid, F. Levy, and G. Burri, Photoluminescence in TiO₂ anatase single crystals, *Solid State Commun.* **87**, 847 (1993).
- [33] H. Tang, H. Berger, P. Schmid, and F. Levy, Optical properties of anatase (TiO₂), *Solid State Commun.* **92**, 267 (1994).
- [34] M. Gallart, T. Cottineau, B. H onerlage, V. Keller, N. Keller, and P. Gilliot, Temperature-dependent photoluminescence of anatase and rutile TiO₂ single crystals: Polar and self-trapped exciton formation, *J. Appl. Phys.* **124**, 133104 (2018).
- [35] S. M. Qaid, M. Hussain, M. Hezam, M. M. Khan, H. Albrithen, H. M. Ghaithan, and A. S. Aldwayyan, Structural and optical investigation of brookite TiO₂ thin films grown by atomic layer deposition on Si (111) substrates, *Mater. Chem. Phys.* **225**, 55 (2019).
- [36] Y. Wang and Y. Li, Template-free preparation and photocatalytic and photoluminescent properties of brookite TiO₂ hollow spheres, *J. Nanomater.* **2019**, 3605976 (2019).
- [37] W. Lamouchi, S. B. Slama, F. Saadallah, and M. Bouaicha, Nickel doping induced amorphization of brookite TiO₂: Photoluminescence enhancement, *Optik* **227**, 166123 (2021).
- [38] J. Zhang, P. Zhou, J. Liu, and J. Yu, New understanding of the difference of photocatalytic activity among anatase, rutile, and brookite TiO₂, *Phys. Chem. Chem. Phys.* **16**, 20382 (2014).
- [39] Y. Zhang, Z. Xing, X. Liu, Z. Li, X. Wu, J. Jiang, M. Li, Q. Zhu, and W. Zhou, Ti³⁺ self-doped blue TiO₂(b) single-crystalline nanorods for efficient solar-driven photocatalytic performance, *ACS Appl. Mater. Interfaces* **8**, 26851 (2016).
- [40] X. Kong, Y. Xu, Z. Cui, Z. Li, Y. Liang, Z. Gao, S. Zhu, and X. Yang, Defect enhances photocatalytic activity of ultrathin TiO₂(b) nanosheets for hydrogen production by plasma engraving method, *Appl. Catal. B* **230**, 11 (2018).
- [41] D. Das and P. Makal, Narrow band gap reduced TiO₂-b: Cu nanowire heterostructures for efficient visible light absorption, charge separation, and photocatalytic degradation, *Appl. Surf. Sci.* **506**, 144880 (2020).
- [42] K. K. Paul, R. Ghosh, and P. Giri, Mechanism of strong visible light photocatalysis by Ag₂O-nanoparticle-decorated monoclinic TiO₂(b) porous nanorods, *Nanotechnology* **27**, 315703 (2016).
- [43] S. Patel and N. Gajbhiye, Intrinsic room-temperature ferromagnetism of V-doped TiO₂(b) nanotubes synthesized by the hydrothermal method, *Solid State Commun.* **151**, 1500 (2011).
- [44] B. Santara, P. Giri, K. Imakita, and M. Fujii, Evidence of oxygen vacancy induced room temperature ferromagnetism in solvothermally synthesized undoped TiO₂ nanoribbons, *Nanoscale* **5**, 5476 (2013).
- [45] N. Siedl, M. J. Elser, E. Halwax, J. Bernardi, and O. Diwald, When fewer photons do more: A comparative O₂ photoadsorption study on vapor-deposited TiO₂ and ZrO₂ nanocrystal ensembles, *J. Phys. Chem. C* **113**, 9175 (2009).
- [46] J. A. Quirk, B. Miao, B. Feng, G. Kim, H. Ohta, Y. Ikuhara, and K. P. McKenna, Unveiling the electronic structure of grain boundaries in anatase with electron microscopy and first-principles modeling, *Nano Lett.* **21**, 9217 (2021).
- [47] D. W. de Quillettes, S. M. Vorpahl, S. D. Stranks, H. Nagaoka, G. E. Eperon, M. E. Ziffer, H. J. Snaith, and D. S. Ginger, Impact of microstructure on local carrier lifetime in perovskite solar cells, *Science* **348**, 683 (2015).
- [48] J. Moseley, W. K. Metzger, H. R. Moutinho, N. Paudel, H. L. Guthrey, Y. Yan, R. K. Ahrenkiel, and M. M. Al-Jassim,

- Recombination by grain-boundary type in CDTE, *J. Appl. Phys.* **118**, 025702 (2015).
- [49] J. Wei, T. Ogawa, B. Feng, T. Yokoi, R. Ishikawa, A. Kuwabara, K. Matsunaga, N. Shibata, and Y. Ikuhara, Direct measurement of electronic band structures at oxide grain boundaries, *Nano Lett.* **20**, 2530 (2020).
- [50] D. Keller, S. Buecheler, P. Reinhard, F. Pianezzi, B. Bissig, R. Carron, F. Hage, Q. Ramasse, R. Erni, and A. N. Tiwari, Band gap widening at random CIGS grain boundary detected by valence electron energy loss spectroscopy, *Appl. Phys. Lett.* **109**, 153103 (2016).
- [51] L. Jing, S. V. Kershaw, T. Kipp, S. Kalytchuk, K. Ding, J. Zeng, M. Jiao, X. Sun, A. Mews, A. L. Rogach *et al.*, Insight into strain effects on band alignment shifts, carrier localization and recombination kinetics in CdTe/CdS core/shell quantum dots, *J. Am. Chem. Soc.* **137**, 2073 (2015).
- [52] L. Dworak, V. V. Matylitsky, V. V. Breus, M. Braun, T. Basché, and J. Wachtveitl, Ultrafast charge separation at the CdSe/CdS core/shell quantum dot/methylviologen interface: Implications for nanocrystal solar cells, *J. Phys. Chem. C* **115**, 3949 (2011).
- [53] C. Li, Y. Wu, J. Poplawsky, T. J. Pennycook, N. Paudel, W. Yin, S. J. Haigh, M. P. Oxley, A. R. Lupini, M. Al-Jassim *et al.*, Grain-Boundary-Enhanced Carrier Collection in CdTe Solar Cells, *Phys. Rev. Lett.* **112**, 156103 (2014).
- [54] M. Zhang, X. Zhang, H.-Q. Lin, and G. Lu, Radiative recombination of large polarons in halide perovskites, *J. Phys.: Condens. Matter* **31**, 165701 (2019).
- [55] D. Ghosh, E. Welch, A. J. Neukirch, A. Zakhidov, and S. Tretiak, Polarons in halide perovskites: A perspective, *J. Phys. Chem. Lett.* **11**, 3271 (2020).
- [56] <https://doi.org/10.15124/79206dfb-5781-4cfd-b6da-7736b92478b7>.
- [57] J. VandeVondele, M. Krack, F. Mohamed, M. Parrinello, T. Chassaing, and J. Hutter, Quickstep: Fast and accurate density functional calculations using a mixed Gaussian and plane waves approach, *Comput. Phys. Commun.* **167**, 103 (2005).
- [58] M. Guidon, J. Hutter, and J. VandeVondele, Robust periodic Hartree-Fock exchange for large-scale simulations using Gaussian basis sets, *J. Chem. Theory Comput.* **5**, 3010 (2009).
- [59] J. Spencer and A. Alavi, Efficient calculation of the exact exchange energy in periodic systems using a truncated coulomb potential, *Phys. Rev. B* **77**, 193110 (2008).
- [60] M. Guidon, J. Hutter, and J. VandeVondele, Auxiliary density matrix methods for Hartree-Fock exchange calculations, *J. Chem. Theory Comput.* **6**, 2348 (2010).
- [61] J. VandeVondele and J. Hutter, Gaussian basis sets for accurate calculations on molecular systems in gas and condensed phases, *J. Chem. Phys.* **127**, 114105 (2007).
- [62] M. Krack, Pseudopotentials for H to Kr optimized for gradient-corrected exchange-correlation functionals, *Theor. Chem. Acc.* **114**, 145 (2005).
- [63] S. Goedecker, M. Teter, and J. Hutter, Separable dual-space Gaussian pseudopotentials, *Phys. Rev. B* **54**, 1703 (1996).
- [64] C. Hartwigsen, S. Goedecker, and J. Hutter, Relativistic separable dual-space Gaussian pseudopotentials from H to Rn, *Phys. Rev. B* **58**, 3641 (1998).